# Beyond Current Guided Bronchoscopy: A Robust and Real-Time Bronchoscopic Ultrasound Navigation System

Xiongbiao Luo and Kensaku Mori

Information and Communications Headquarters, Nagoya University
xiongbiao.luo@gmail.com, kensaku@is.nagoya-u.ac.jp

**Abstract.** This paper develops a new bronchoscopic ultrasound navigation system that fuses multimodal sensory information including pre-operative images, bronchoscopic video sequences, ultrasound images, and external position sensor measurements. To construct such a system, we must align these information coordinate systems. We use hand-eye calibration to align the video camera and its attached external sensor and introduce a phantom-free method to calibrate the ultrasonic probe and its fixed external sensor. More importantly, we propose a marker-free registration method that uses the bronchoscope and the bronchial tree center information to register the sensor and the pre-operative coordinate systems. We constructed a bronchial phantom to validate our system, whose navigation accuracy was about 2.6 mm. Furthermore, compared to the current navigated bronchoscopy, the main advantage of our system is that it navigates the bronchoscope and the ultrasonic mini probe simultaneously and provides bronchial structures inside and outside the bronchial walls, particularly lymph node structures in ultrasonic images.

## 1 Introduction

Guided bronchoscopy fuses different modal sensory information to assist physicians to perform endoscopic interventions, e.g., transbronchial lung biopsy (TBLB) for lung cancer staging. Numerous papers have discussed guided bronchoscopy in the literature. Image registration (IR) methods are widely used in guided bronchoscopy [1,2], although they still suffer from problematic video images, e.g., surface mucus. Electromagnetic tracking (ET) systems are increasingly employed in bronchoscopic navigation [3,4,5]. Both IR- and ET-based techniques navigate the bronchoscope well to the target regions. After reaching the suspicious regions, fluoroscopy must be performed to guide the tissue biopsies since biopsy needles cannot be observed in the suspicious regions beyond the bronchial walls from the CT and video images [3]. The ultrasound mini probe is a promising device to observe needles and structures beyond bronchial walls in ultrasound images [6]. However, it cannot navigate itself to targets during interventions.

Beyond current guided bronchoscopy that performs biopsies with fluoroscopy, we construct a real-time bronchoscopic ultrasound guidance system that can navigate a bronchoscope and a ultrasound mini probe simultaneously and observe

K. Mori et al. (Eds.): MICCAI 2013, Part I, LNCS 8149, pp. 388–395, 2013.

biopsy needles and pulmonary structures beyond the bronchial walls. Our system combines bronchoscopic video, an ultrasound probe, an ET system, and CT slices to navigate the bronchoscope and the probe and guide the bronchoscopic accessory tools. To establish different alignments in our system, we propose phantom-free and marker-free registration methods after hand-eye calibration.

The contribution of this work is threefold. To the best of our knowledge, no guided bronchoscopy systems have been reported that resemble our system. Our system can track not only the bronchoscope and the ultrasound probe synchronously but it can also observe endoscopic accessory tools and pulmonary structure without fluoroscopy. We propose an improved marker-free registration approach to align an external tracking sensor and pre-operative images. Our method, which uses both bronchoscope and bronchial tree center information, was demonstrated to be more accurate than the others. Additionally, we introduce phantom-free calibration to align the ET and ultrasound systems.

## 2 Navigation System Design

### 2.1 Hardware

Our system includes the following hardware: (1) an ET system and two electromagnetic sensors (ES), (2) an ultrasound (US) miniature radial probe, (3) a bronchoscopic camera (BC) integrated into a bronchoscope in an endoscopy system, and (4) a host computer with an user interface display. We use an ET system with two sensors fixed to collect bronchoscope and US miniature probe movements. Additionally, we need to acquire the CT images of the anatomy. In general, our system involves five coordinate spaces: ET, ES, BS, US, and CT (Fig. 2).

### 2.2 Software

We designed our system interface with five displays: (1) unmodified and real-time bronchoscopic video, (2) axial view of reformatted CT slices, synchronized with video and US images, (3) unchanged and real-time US images, (4) real-time virtual rendering images that correspond to video and US sequences, and (5) segmented three-dimensional lung structures that include airway trees and lymph nodes and real-time US images that are transformed in the CT space.

## 3 Approaches in Navigation

To realize our navigation system, we determine four transformations, ${}^{ES_1}\mathbf{T}_{BC}$, ${}^{ES_2}\mathbf{T}_{US}$, ${}^{CT}\mathbf{T}_{ET}$, and ${}^{CT}\mathbf{T}_{US}$, among five coordinate systems: ET, ES, BS, US, and CT. Two sensor outputs, ${}^{ET}\mathbf{T}_{ES_1}$ (to record the bronchoscope motion) and ${}^{ET}\mathbf{T}_{ES_2}$ (to measure the US probe motion), indicate the transformation between the ET and ES coordinate systems. We must determine these transformations of ${}^{ES_1}\mathbf{T}_{BC}$, ${}^{ES_2}\mathbf{T}_{US}$, ${}^{CT}\mathbf{T}_{ET}$, and ${}^{CT}\mathbf{T}_{US} = {}^{CT}\mathbf{T}_{ET}{}^{ET}\mathbf{T}_{ES_2}{}^{ES_2}\mathbf{T}_{US}$ to navigate the bronchoscope and the US probe in our system. We propose phantom-free and marker-free methods for obtaining ${}^{ES_2}\mathbf{T}_{US}$ and ${}^{CT}\mathbf{T}_{ET}$.

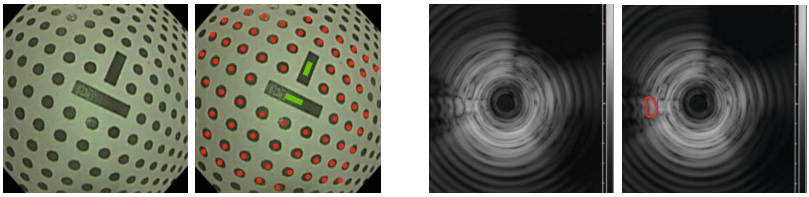

(a) Detected pattern image (b) Detected US image

**Fig. 1.** Images for BC-ES spatial alignment and phantom-free US-ES calibration

### 3.1 BC-ES Spatial Alignment

To compute ${}^{ES_1}\mathbf{T}_{BC}$, we perform a hand-eye calibration, which establishes the hand (e.g., a robot gripper) and eye (e.g., a camera) relationship that can be calculated using a number of acquired camera and gripper motions. In our case, "*hand*" corresponds to the ET sensor, and "*eye*" relates to the bronchoscope camera. Using pattern images (Fig. 1 (a)), ${}^{ES_1}\mathbf{T}_{BC}$ can be solved by [7]:

$$\begin{cases} \Delta^{ES_1}\mathbf{T}_{ij} \cdot {}^{ES_1}\mathbf{T}_{BC} = {}^{ES_1}\mathbf{T}_{BC} \cdot \Delta^{BC}\mathbf{T}_{ij} \\ \Delta^{ES_1}\mathbf{T}_{ij} = {}^{ES_1}\mathbf{T}^{i}_{ET} \cdot {}^{ET}\mathbf{T}^{j}_{ES_1} \\ \Delta^{BC}\mathbf{T}_{ij} = {}^{BC}\mathbf{T}^{i}_{P} \cdot {}^{P}\mathbf{T}^{j}_{BC} \end{cases}, \tag{1}$$

where $\Delta^{ES_1}\mathbf{T}_{ij}$ is the relative sensor motion measured by the EM system and $\Delta^{BC}\mathbf{T}_{ij}$ is the camera movement relative to the calibration pattern frame for the bronchoscope moving from the $i$-th pose to the $j$-th pose. Bronchoscopic camera pose ${}^{BC}\mathbf{T}^{i}_{P}$ is computed by the camera calibration [7].

### 3.2 Phantom-Free US-ES Calibration

We here propose a phantom-free method to calculate ${}^{ES_2}\mathbf{T}_{US}$. Since we attach an ET sensor to the US probe, the sensor shape can be observed in the US images (Fig. 1(b)). We segment such a shape and get its center point $\mathbf{a}^{us}_k$ that is represented by homogeneous coordinates: $\mathbf{a}^{us}_k = (a^x_k, a^y_k, 0, 1)^T$ ($k$ indicates the US frame number). We perform the following minimization to compute ${}^{ES_2}\mathbf{T}_{US}$:

$${}^{ES_2}\tilde{\mathbf{T}}_{US} = \arg\min_{{}^{ES_2}\mathbf{T}_{US}} \left\| \mathbf{p}_k - {}^{ET}\mathbf{T}_{ES_2} \cdot {}^{ES_2}\mathbf{T}_{US} \cdot \mathbf{a}^{us}_k \right\|, \tag{2}$$

where position $\mathbf{p}_k = (p^x_k, p^y_k, p^z_k, 1)^T$ is from the sensor attached at the US probe.

### 3.3 Real-Time Marker-Free ET-CT Registration

Since the accuracy of our system is heavily influenced by the ET-CT registration error, we modify the marker-free method to compute ${}^{CT}\mathbf{T}_{ET}$ more accurately. To synchronize the ET and CT coordinate systems, we could use either the marker-based or marker-free methods [3,5]. Although the marker-based method

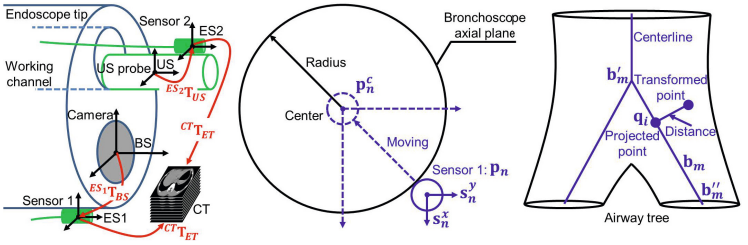


**Fig. 2.** Coordinate systems involved in our navigation system (*left*), moving original sensor position $\mathbf{p}_n$ to bronchoscope center $\mathbf{p}_n^c$ (*middle*), and assigning bronchus centerline $\mathbf{b}_m$ to modified sensor position $\mathbf{p}_n^c$ (*right*)

works well [3], it is somewhat difficult to perform it operating rooms. Without additional setups (e.g., anatomical marker selection), the marker-free method assumes that the bronchoscope is operated along the bronchial centerlines in the bronchoscopy; such an assumption is easily violated in practice.

To address the above assumption, we move the sensor measurements much closer to the bronchial centerlines. We believe that the center of the bronchoscope axial plane is closer to the bronchial centerlines than the position of the sensor attached to the bronchoscope surface. Therefore, we can move the sensor measurement to the center of the bronchoscope axial plane (Fig. 2). Changing the sensor position to the bronchoscope center (close to the bronchial centerlines) will prove very effective in our experiments.

Suppose $(\mathbf{p}_n, \mathbf{s}_n^x, \mathbf{s}_n^y, \mathbf{s}_n^z)$ (i.e., ${}^{ET}\mathbf{T}_{ES_1}$) is the measurement with position $\mathbf{p}_n$ and the orientation $(\mathbf{s}_n^x, \mathbf{s}_n^y, \mathbf{s}_n^z)$ of the $x$-, $y$-, and $z$-directions from the sensor is attached to the bronchoscope surface ($n$ is the measurement number). Based on sensor output directions $\mathbf{s}_n^x$ and $\mathbf{s}_n^y$, bronchoscope center $\mathbf{p}_n^c$ is calculated by:

$$\mathbf{p}_n^c = \mathbf{p}_n - r_b \cdot (\mathbf{s}_n^x + \mathbf{s}_n^y), \tag{3}$$

where $r_b$ is the bronchoscope radius. Fig. 2 shows the relation of $\mathbf{p}_n^c$ and $\mathbf{p}_n$. After we segment the CT images to get bronchial centerline $\mathbf{b}_m = (\mathbf{b}_m^{'}, \mathbf{b}_m^{''})$ ($m$ is the bronchus number, $\mathbf{b}_m^{'}$ and $\mathbf{b}_m^{''}$ are the start and end points of $\mathbf{b}_m$), we assign closest centerline $\hat{\mathbf{b}}_m$ to $\mathbf{p}_n^c$ by minimizing distance $E({}^{CT}\mathbf{T}_{ET} \cdot \mathbf{p}_n^c, \mathbf{b}_m)$:

$$\hat{\mathbf{b}}_m = \arg\min_{\mathbf{b}_m} E({}^{CT}\mathbf{T}_{ET} \cdot \mathbf{p}_n^c, \mathbf{b}_m), \tag{4}$$

where ${}^{CT}\mathbf{T}_{ET} \cdot \mathbf{p}_n^c$ is the transformed point and $E({}^{CT}\mathbf{T}_{ET} \cdot \mathbf{p}_n^c, \mathbf{b}_m)$ is defined as (Fig. 2)

$$\mathbf{E}({}^{CT}\mathbf{T}_{ET} \cdot \mathbf{p}_n^c, \mathbf{b}_m) = \begin{cases} ||{}^{CT}\mathbf{T}_{ET} \cdot \mathbf{p}_n^c - \mathbf{b}_m^{'}|| & \lambda < 0 \\ ||{}^{CT}\mathbf{T}_{ET} \cdot \mathbf{p}_n^c - \mathbf{b}_m^{''}|| & \lambda > ||\mathbf{b}_m^{''} - \mathbf{b}_m^{'}|| \\ \sqrt{||{}^{CT}\mathbf{T}_{ET} \cdot \mathbf{p}_n^c - \mathbf{b}_m^{'}||^2 - \lambda^2} & otherwise \end{cases}, \tag{5}$$

where $\lambda = ({}^{CT}\mathbf{T}_{ET} \cdot \mathbf{p}_n^c - \mathbf{b}_m^{'}) \cdot (\mathbf{b}_m^{''} - \mathbf{b}_m^{'}) \cdot ||\mathbf{b}_m^{''} - \mathbf{b}_m^{'}||^{-1}$. Since we might obtain several centerlines $\{\hat{\mathbf{b}}_m\}$, we choose optimal centerline $\mathbf{b}_{m*}$ by computing the difference between vector $(\hat{\mathbf{b}}_m^{''} - \hat{\mathbf{b}}_m^{'}) \cdot ||\hat{\mathbf{b}}_m^{''} - \hat{\mathbf{b}}_m^{'}||^{-1}$ and sensor $z$-direction $\mathbf{s}_n^z$:

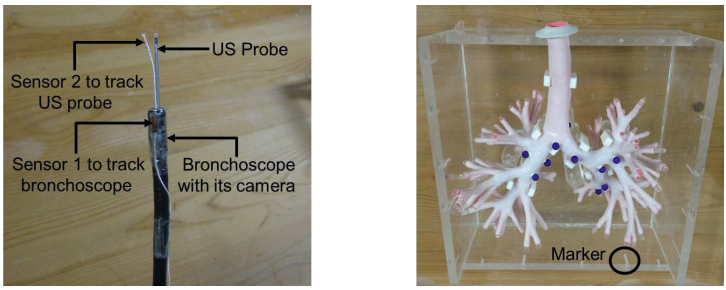


**Fig. 3.** Sensor, bronchoscope, US probe, and phantom used in experiments

$$\mathbf{b}_{m*} = \arg\min_{\{\hat{\mathbf{b}}_m\}} \arccos < \frac{\hat{\mathbf{b}}_m^{''} - \hat{\mathbf{b}}_m^{'}}{||\hat{\mathbf{b}}_m^{''} - \hat{\mathbf{b}}_m^{'}||}, \quad \frac{{}^{CT}\mathbf{T}_{ET} \cdot \mathbf{s}_n^z}{||{}^{CT}\mathbf{T}_{ET} \cdot \mathbf{s}_n^z||} >, \tag{6}$$

where $<,>$ represents the dot product. We project transformed point ${}^{CT}\mathbf{T}_{ET} \cdot \mathbf{p}_n^c$ on optimal centerline $\mathbf{b}_{m*}$ and obtain projected point $\mathbf{q}_n$ (Fig. 2):

$$\mathbf{q}_n = \mathbf{b}_{m*}^{'} + \frac{({}^{CT}\mathbf{T}_{ET} \cdot \mathbf{p}_n^c - \mathbf{b}_{m*}^{'}) \cdot (\mathbf{b}_{m*}^{''} - \mathbf{b}_{m*}^{'})}{||\tilde{\mathbf{B}}_i^{''} - \tilde{\mathbf{B}}_i^{'}||} \cdot \frac{(\mathbf{b}_{m*}^{''} - \mathbf{b}_{m*}^{'})}{||\mathbf{b}_{m*}^{''} - \mathbf{b}_{m*}^{'}||}. \tag{7}$$

Finally, we obtain bronchoscope center points $\mathcal{M} = \{(\mathbf{p}_n^c, \mathbf{s}_n^x, \mathbf{s}_n^y, \mathbf{s}_n^z)\}_{n=1}^N$ and projected points $\mathcal{P} = \{\mathbf{q}_n\}_{n=1}^N$ (total sensor measurement number $N$) and determine optimal ${}^{CT}\tilde{\mathbf{T}}_{ET}$ by ($r_{m*}$ is the radius of $\mathbf{b}_{m*}$):

$${}^{CT}\tilde{\mathbf{T}}_{ET} = \arg\min_{\mathbf{p}_n^c \in \mathcal{M}, \mathbf{q}_n \in \mathcal{P}} \sum_n \frac{||{}^{CT}\mathbf{T}_{ET} \cdot \mathbf{p}_n^c - \mathbf{q}_n||}{r_{m*}}. \tag{8}$$

## 4 Navigation Accuracy Analysis

**Experimental Settings** In our experiments, we used a 3-D Guidance medSAFE tracker (Ascension Technology Corporation, USA) as our ET system. Two electromagnetic sensors (1.5 mm, 6DoF) were attached to a bronchoscope (BF Type 200, Olympus, Tokyo) and US probe (UM-S20-17S, Olympus, Tokyo) for tracking their movements (Fig. 3). The tip diameter of the bronchoscope and the probe was 4.0 and 1.7 mm. We constructed a bronchial phantom to evaluate our methods. Its CT space parameters were $512 \times 512 \times 611$ voxels and $0.892 \times 0.692 \times 0.5$ mm$^3$. We placed twenty markers on the phantom (Fig. 3) and used them to evaluate the registration error of ${}^{CT}\mathbf{T}_{ET}$ by: $Err = \sum_{o=1}^{20} ||\mathbf{q}_o^{CT} - {}^{CT}\mathbf{T}_{ET} \cdot \mathbf{p}_o^{ET}||/20$.

**Accuracy Analysis.** Our constructed system interface with five displays (Fig. 4) provides physicians with different visualization information. We used twelve pattern images with twelve sensor measurements to perform the hand-eye calibration. The calibration error was about 0.5 mm. We also used ten frames of US

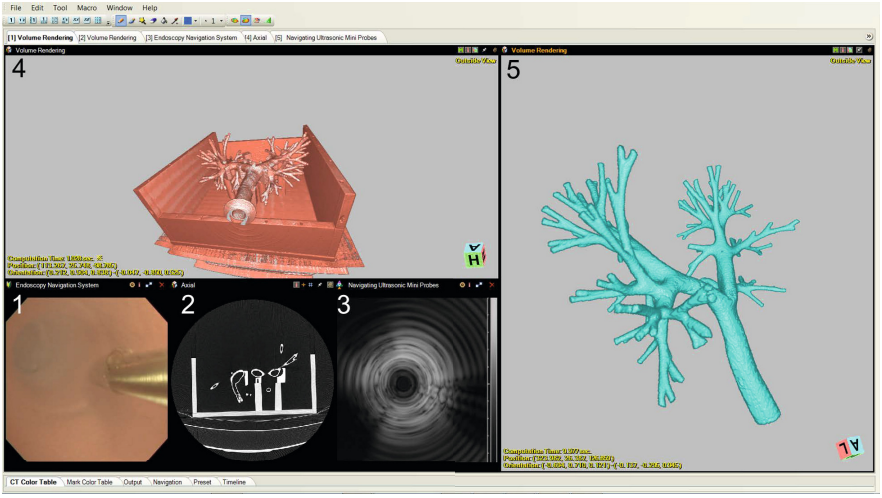


**Fig. 4.** Our system interface with five displays: 1, 2, 3, 4, and 5

**Table 1.** Quantitative comparison of average registration error and average distance (Eq. 5) between sensor measurements and bronchial centerlines

| Methods | Deguchi et al. [5] | | Our method | |
|---|---|---|---|---|
| Experiments | Accuracy | Distance | Accuracy | Distance |
| 1 | 6.9 mm | 5.2 mm | 3.2 mm | 4.2 mm |
| 2 | 4.0 mm | 5.1 mm | 2.6 mm | 4.1 mm |
| 3 | 3.9 mm | 4.8 mm | 1.4 mm | 3.9 mm |
| 4 | 4.8 mm | 5.2 mm | 2.9 mm | 4.2 mm |
| 5 | 4.9 mm | 6.1 mm | 3.1 mm | 3.1 mm |
| **Average** | **4.9 mm** | **5.3 mm** | **2.6 mm** | **3.9 mm** |

images to align the US and sensor coordinate systems. The current alignment error was around 0.8 mm. Table 1 quantifies the average ET-CT registration error and the average distance (computed by Eq. 5) between the sensor measurements and the bronchial centerlines in the five experiments. The distance to the bronchial centerlines of the methods of Deguchi et al. [5] and ours was around 5.3 and 3.9 mm. The average registration error was reduced from 4.9 to 2.6 mm. Fig. 5 shows the registration accuracy, the distance, and the sensor measurement points distributed inside the bronchial trees of Experiment 5. Fig. 6 compares the registration results of the two methods. Since the virtual images generated from the registered results of our method more closely resemble the video images than Deguchi et al. [5], our method outperforms it [5].

Compared with current guided bronchoscopy, we believe that our system is promising since it provides different visualization information, e.g., the current bronchoscope and US probe positions in the CT coordinate system and the pulmonary structures and the biopsy needle locations inside and outside the bronchial walls, to assist physicians to perform bronchoscopic interventions. We

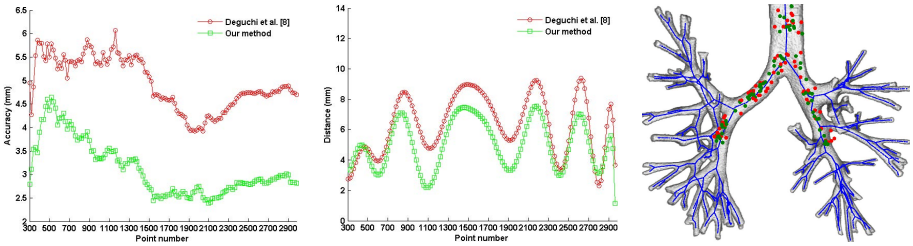


**Fig. 5.** Plotted registration accuracy (*left*) and distance to bronchial centerlines (*middle*). *Right*: *Green* points based on our method were closer to *blue* bronchial centerlines than *red* points generated from Deguchi et al. [5]

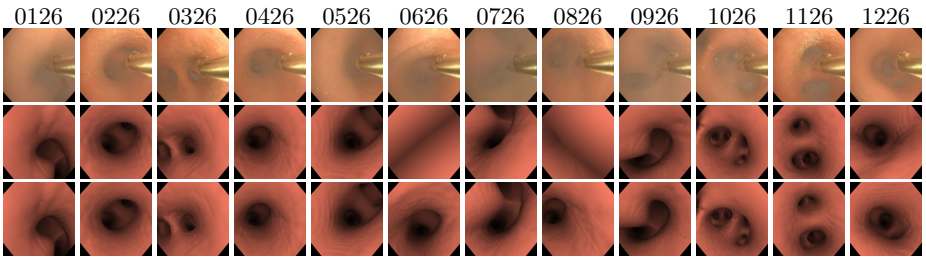


**Fig. 6.** Visual comparison of ET-CT registration results. Top row shows uniformly selected frame numbers, and second row shows their corresponding video images. Third and fourth rows display virtual images registered by Deguchi et al. [5] and our method. Our method shows better performance.

also improved the registration accuracy of the marker-free method. We attribute such an improvement to moving the original sensor position to the bronchoscope center to reduce the distance between the sensor positions and the bronchial centerlines (Fig. 5). Our experimental results demonstrated that our idea can significantly diminish the assumption of moving the bronchoscope along the bronchial centerlines. However, our system navigation error still originated mainly from the ET-CT registration step due to static and dynamic errors of our ET system. The inherent static error is 1.4 mm. The dynamic error, which is difficult to correct without optical trackers, is caused by the dynamic magnetic field distortion that results from metals in the working volume of our ET system. Note that, in our current validation, we did not consider the respiratory motion problem, which also challenges our system's navigation accuracy. It is possible to track the breathing motion by attaching several sensors to the thorax to compensate the accuracy. We will evaluate our method on patient datasets or a dynamic phantom that can simulate breathing motion in the future.

## 5 Conclusions

This paper proposed a new bronchoscopic ultrasound navigation system that combines pre-operative images, bronchoscopic video sequences, ultrasound images, and external position sensor measurements. The most advantageous point of our system enables physicians to navigate the bronchoscope and the ultrasonic mini probe simultaneously, locating bronchial structures inside and outside the bronchial walls in the video and US images, particularly pulmonary lymph nodes where biopsies may be performed. We also modified a marker-free method to perform CT-to-physical registration on the basis of moving sensor positions to the bronchoscope axial centers. The current registration accuracy can be improved from 4.9 to 2.6 mm, which approximates the clinical requirement of 2.0 mm. Future work includes further improvement of our system navigation accuracy under respiratory motion and validating our system on patient datasets.

**Acknowledgment.** This work was partly supported by the center of excellence project "Development of high-precision bedside devices for early metastatic cancer diagnosis and surgery" (01-D-D0806) funded by the Aichi Prefecture, the JSPS Kakenhi "Modality-seamless navigation for endoscopic diagnosis and surgery assistance based on multi-modality image fusion" (25242047), and the project "Computational anatomy for computer-aided diagnosis and therapy: frontiers of medical image sciences" (21103006) funded by a Grant-in-Aid for Scientific Research on Innovative Areas, MEXT, Japan.

## References

1. Deligianni, F., Chung, A.J., Yang, G.Z.: Nonrigid 2-D/3-D registration for patient specific bronchoscopy simulation with statistical shape modeling: Phantom validation. IEEE TMI 25(11), 1462–1471 (2006)
2. Luo, X., Feuerstein, M., Deguchi, D., Kitasaka, T., Takabatake, H., Mori, K.: Development and comparison of new hybrid motion tracking for bronchoscopic navigation. MedIA 16(3), 577–596 (2012)
3. Schwarz, Y., Greif, J., Becker, H.D., Ernst, A., Mehta, A.: Real-time electromagnetic navigation bronchoscopy to peripheral lung lesions using overlaid CT images: The first human study. Chest 129(4), 988–994 (2006)
4. Luo, X., Kitasaka, T., Mori, K.: Bronchoscopy navigation beyond electromagnetic tracking systems: a novel bronchoscope tracking prototype. In: Fichtinger, G., Martel, A., Peters, T. (eds.) MICCAI 2011, Part I. LNCS, vol. 6891, pp. 194–202. Springer, Heidelberg (2011)
5. Deguchi, D., Feuerstein, M., Kitasaka, T., Suenaga, Y., Ide, I., Murase, H., Imaizumi, K., Hasegawa, Y., Mori, K.: Real-time marker-free patient registration for electromagnetic navigated bronchoscopy: a phantom study. IJCARS 7(3), 359–369 (2012)
6. Herth, F.J.F., Schuler, H., Gompelmann, D., Kahn, N., Gasparini, S., Ernst, A., Schuhmann, M., Eberhardt, R.: Endobronchial ultrasound-guided lymph node biopsy with transbronchial needle forceps: a pilot study. Eur. Respir. J. 39, 373–377 (2012)
7. Wengert, C., Reeff, M., Cattin, P.C., Szekely, G.: Fully automatic endoscope calibration for intraoperative use. In: BFDM 2006, pp. 419–423. Springer (2006)